ACS APPLIED MATERIALS & INTERFACES

www.acsami.org

Research Article

Electrostatic Self-Assembly-Driven Heterojunction of Cubic CeO_2/g-C_3N_4 Nanosheets for Efficient Photocatalytic Hydrogen Evolution and Photoelectrocatalytic Water Splitting: A Hybrid Experimental and Theoretical Study

Abinash Das,* Shriya Gumber, Nitai C. Maji, Shashi B. Mishra,* Preethi M., Pujita Ningthoukhongjam, Ranjith G. Nair, Abhijith T., Elena A. Kazakova, Andrey S. Vasenko, Madhumitha R., and Oleg V. Prezhdo*

Cite This: https://doi.org/10.1021/acsami.5c10272

Read Online

ACCESS | Metrics & More | Article Recommendations | Supporting Information

ABSTRACT: Nanohybrid catalysts hold great promise for photocatalysis and photoelectrocatalysis, with significant progress still to be made. We synthesize a graphitic carbon nitride (GCN)−CeO_2 heterojunction via electrostatic self-assembly. Characterization confirms that CeO_2 nanocubes are uniformly anchored onto layered GCN, forming a high-quality interface with abundant active sites. This architecture facilitates efficient separation of photogenerated charge carriers and an improved optical response, as further supported by density functional theory and finite-difference time-domain simulations, which reveal a modified band structure and optical response at the type-II heterojunction interface. The resulting hybrid exhibits excellent water splitting performance, with a photocurrent density of 5.70 mA cm^{-2} at a low onset potential of 0.43 V vs Ag/AgCl. The GCN−CeO_2 photocatalyst shows an enhanced hydrogen evolution rate of 809.23 μmol g^{-1} h^{-1}, which is 6.7 times higher than that of pure CeO_2 and 3.2 times higher than that of the GCN photocatalyst. The reported findings highlight the promising potential of electrostatic self-assembly as an effective strategy for the development of efficient catalysts for solar fuel production.

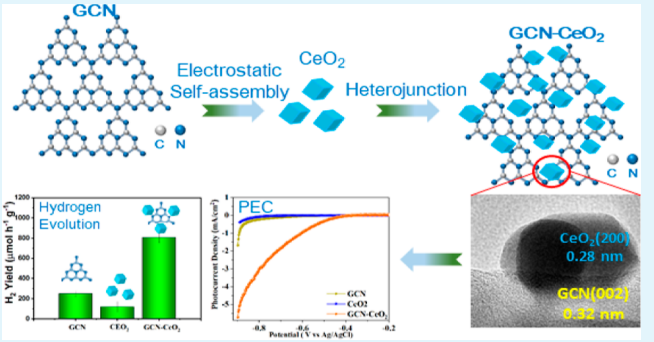

KEYWORDS: *photocatalysis, photoelectrocatalysis, green hydrogen, 2D materials, self-assembly, heterojunction, water splitting*

1. INTRODUCTION

Hydrogen has been considered as a clean and carbon-free fuel for the sustainable future. However, hydrogen production is primarily dependent on steam reforming methods, which cause an eventual depletion of fossil fuels and CO_2 emissions. Therefore, catalytic water splitting to produce hydrogen via photoelectrocatalysis and photocatalysis represents a green solution for addressing the global energy demand.[1−4] One of the key factors associated with this technology is the development of efficient photoactive catalysts. Over the past few decades, significant efforts have been made to optimize catalysts to construct efficient catalytic systems. Several types of photoactive materials have been investigated so far, such as metal oxides, sulfides, layered materials, perovskites, and organic polymers.[5−7] Recently, ultrathin carbon nitride with graphite-phase (g-C_3N_4), especially the single-/few-layered 2D structure, has been considered as an outstanding catalyst for water splitting.[8−10] g-C_3N_4 is a metal-free carbon- and nitrogen-rich compound. It has earned strong attention as a potential catalyst since its first report in 2009.[11,12] g-C_3N_4 exhibits a reasonable band gap value between 2.4 and 2.8 eV and also has high chemical and thermal stability.[13] Even though the light harvesting capacity of g-C_3N_4 corresponds to the visible region, catalytic performance of pristine g-C_3N_4 is not very promising due to poor optical properties, low charge carrier lifetime, and low surface area of bulk g-C_3N_4.[14−16] Various strategies have been explored in order to address these shortcomings, such as doping, sensitization, tuning different precursors, and exfoliation into thin 2D layers.[8,17] In addition to these strategies, constructing a heterojunction with g-C_3N_4 by coupling with other semiconductors has emerged as an

Received: May 25, 2025
Revised: July 3, 2025
Accepted: August 8, 2025

effective approach to improve the lifetime of photoinduced charge carriers.[18,19] Extensive research efforts have been dedicated to strategies for maximizing the efficiency of g-C_3N_4 by coupling it with WO_3, Fe_2O_3, ZnO, TiO_2, and other metal oxides, which involve earth-abundant elements and are stable in water.[20−23]

Recently, rare-earth-element-based oxides have been considered as counterparts of g-C_3N_4 to improve its photoactivity. Cerium dioxide (CeO_2) is considered as the ideal counterpart to form a heterojunction with g-C_3N_4 because of its suitable band edge position and the reversible redox Ce(IV)/Ce(III) state couple, which can control the photoelectrochemical (PEC) and photocatalytic performance of the hybrid catalyst.[24−26] It has been found that the reversible conversion of the Ce(IV)/Ce(III) states can ensure efficient charge transfer through the interface of the heterojunction, thereby benefiting catalytic activity. To date, several combinations, such as ZnO@CeO_2, rGO@CeO_2, and MoS_2@cubic−CeO_2, have been reported in the catalytic water splitting applications.[27,28] The optical and structural properties of these heterojunctions are improved compared to the pristine system. However, the preparation of the heterojunctions is always complex and often requires dedicated templates and time-consuming processes. These reports have indicated that the presence of CeO_2 in the heterojunction materials is beneficial for boosting the light harvesting capacity, charge transfer rate, and electron−hole pair separation. The modifications may arise from the complementary synergy between the two materials and their suitable band alignments with good lattice matching. Thus, coupling CeO_2 with g-C_3N_4 to form a stable heterojunction constitutes a promising strategy to obtain a high catalytic performance. Both carbon-based materials, such as g-C_3N_4, and metal oxides, such as CeO_2, have been integrated into perovskite solar cells to improve stability, enhance charge transport, and reduce charge recombination.[29,30] Combinations of perovskites with CeO_2/g-C_3N_4 composites provide further routes for improved photocatalytic water splitting.

The g-C_3N_4/CeO_2 composites can be obtained by using several techniques, such as in situ coupling, physical mixing, ball milling, and thermal polycondensation. These approaches primarily utilize g-C_3N_4 to host CeO_2. Other approaches include (a) sonication or hydrothermal-based treatment in the presence of preformed CeO_2 and g-C_3N_4 in organic solvents or water; (b) formation of CeO_2 in the presence of nitrogen-rich precursors such as urea, melamine, thiourea, etc.; and (c) formation of g-C_3N_4 in the presence of Ce-based salts.[31,32] Most of these methods cannot ensure a uniform nanoparticle dispersion and strong interfacial contact. Recently, Chauhan and Gupta have reported fabrication of a g-C_3N_4/CeO_2 composite using the hydrothermal method.[33] Similarly, Tripathi et al. have coupled CeO_2 with g-C_3N_4 through in situ copyrolysis of the cerium-based complex and melamine, followed by acidification and exfoliation of the composite.[34] Li et al. have reported development of a CeO_2/g-C_3N_4 composite using ultrasonic impregnation for catalytic degradation of phenanthrene.[35] Noticeably, these approaches are suitable for laboratory studies, while they are less ideal for large-scale fabrication as they involve time-consuming and complex steps.

There have been few reports in which the heterojunction is formed through the manipulation of the surface charge of CeO_2 and g-C_3N_4. This approach is scalable, simple, and less time-consuming. In general, it is challenging to control the interfacial contact between layered g-C_3N_4 nanosheets and cocatalysts, which results in a nonuniform integration and poor interfacial contact, leading to unsatisfactory photoactivity. Hence, it is essential to develop a low-cost and simple method to effectively design an intimate contact between 2D *g*-C_3N_4 nanosheets and its counterpart for improved catalytic performance. In this context, the electrostatic self-assembly process can be a suitable method to create a high-quality interface between the 2D nanosheet and CeO_2 for a stable heterojunction. Moreover, attributed to the simplicity in composition, controllability, and being unconstrained by lattice matching, strong electrostatic adherence can be created by manipulating the surface charge alone, which will induce better alignment within the heterostructure.[36−38]

In this work, we combine oppositely charged CeO_2 and ultrathin g-C_3N_4 to construct a uniform catalytic heterojunction through electrostatic self-assembly and demonstrate a multifunctional application of the heterojunction catalyst. The optimal catalyst shows high catalytic activity for photocatalytic hydrogen production and PEC water splitting. The heterojunction catalysts are also studied through DFT calculations[39−41] to examine the modified optical and electronic properties of the catalyst activated through electrostatic self-assembly. The method involved in the electrostatic self-assembly is explained by the zeta potential calculation of the particle suspension. The evaluated photocatalytic and PEC performances of the samples demonstrate that the g-C_3N_4 layer decorated with cubic CeO_2 shows significantly improved activity, indicating that not only the material properties but also the intimate interactions between the particle surfaces play a crucial role in the photocatalytic water splitting and related applications.

2. EXPERIMENTAL SECTION

2.1. Materials and Methods. Urea (99.5%, Loba Chemie), cerium(III) nitrate hexahydrate $Ce(NO_3)_3{\bullet}6H_2O$ (99.00%, HIMEDIA), sodium hydroxide (Merck, India), and sulfuric acid (Merck, India) were procured and used as received. Deionized water and ethanol (99.9%) were used as solvents throughout the experiment.

For the synthesis of g-C_3N_4, 15 g of urea was taken in a silica crucible and kept in a programmable Muffle Furnace at 500 °C for 2 h (ramping rate of 7 °C/min). As a result, yellow particles of g-C_3N_4 were obtained and kept for further use. On the other hand. The CeO_2 nanocube was obtained using the hydrothermal method. Initially, $Ce(NO_3)_3{\cdot}6H_2O$ (4 mmol) and NaOH (96 mmol) were dissolved in deionized water (20 and 30 mL, respectively). Then, the $Ce(NO_3)_3{\cdot}6H_2O$ solution was added slowly to the NaOH solution and stirred for 30 min at room temperature, followed by sonication for 30 min to get a purple slurry. The purple slurry was transferred to a 100 mL Teflon-lined stainless-steel autoclave and heated at 160 °C for 24 h. The precipitate was then washed with deionized water and ethanol to obtain the pure sample; later, the precipitate was dried in a hot air oven to obtain the powder sample. Finally, the CeO_2 powder was calcined at 600 °C for 3 h to obtain heterogeneous nanocube-like structures of CeO_2.

2.1.1. Zeta Potential Measurement and Electrostatic Self-Assembly. In order to obtain heteroaggregation of two oppositely charged particles, a total of 4 dispersions were prepared at different pH values, ranging from 3 to 9, as shown in Figure S1. The zeta potential of g-C_3N_4 and CeO_2 particles can be tuned by adjusting the pH of the dispersion at different pH values, and the consistency of the results was confirmed from three repeated measurements. In order to obtain an electrostatic self-assembly-driven heterojunction, it is essential to identify the surface charge or the zeta potential of the particles as a function of pH. The pH value over which g-C_3N_4 and CeO_2 are oppositely charged can form a heterojunction. g-C_3N_4 and

https://doi.org/10.1021/acsami.5c10272
ACS Appl. Mater. Interfaces XXXX, XXX, XXX−XXX

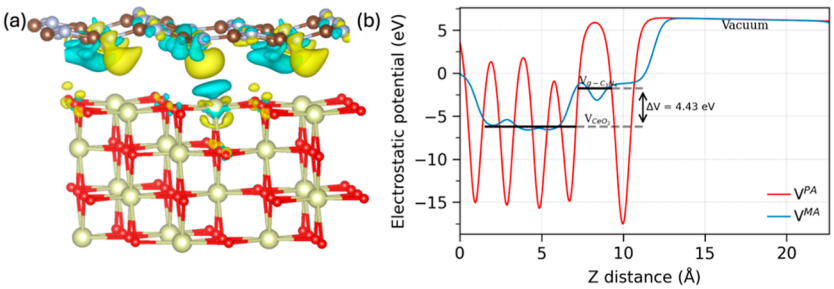

Figure 11. (a) Charge density difference (CDD) plot of the $CeO_2(110)/g\text{-}C_3N_4$ heterostructure. Yellow and cyan iso-surfaces represent regions of charge accumulation and depletion, respectively, with an iso-value of 0.001 eV/Å^3. (b) Plane-averaged electrostatic potential ($V^{(PA)}$, red) and macroscopic-averaged electrostatic potential ($V^{(MA)}$, blue) along the z-direction. The potential step ($\Delta V \approx 4.43$ eV) between the g-C_3N_4 and CeO_2 regions indicates interfacial dipole formation and supports type-II band alignment.

of combining wide- and narrow-gap semiconductors enhances photoactivity.[60]

To further understand the interfacial charge transfer, we calculated the charge density difference (CDD) using the expression $\Delta\rho = \rho_{CeO_2(110)/g\text{-}C_3N_4} - \rho_{CeO_2} - \rho_{g\text{-}C_3N_4}$, where $\rho_{CeO_2(110)/g\text{-}C_3N_4}$, ρ_{CeO_2}, and $\rho_{g\text{-}C_3N_4}$ represent the charge densities of the heterostructure, the isolated $CeO_2(110)$ surface, and the g-C_3N_4 layer, respectively. Figure 11a,b shows the CDD and electrostatic potential profiles across the $CeO_2(110)/g\text{-}C_3N_4$ heterostructure. The planar-averaged and macroscopic-averaged electrostatic potential profiles were calculated following the procedures described in the prior literature,[46,74,75] helping quantify the interfacial potential steps and dipole formation. The CDD plot reveals a charge redistribution at the interface, with the yellow and cyan isosurfaces indicating charge accumulation and depletion, respectively. This asymmetric redistribution suggests formation of interfacial polarization and charge transfer from the $CeO_2(110)$ surface to the g-C_3N_4 layer, driven by differences in work function and electron affinity. The electrostatic potential profiles along the z-direction exhibit a significant potential step ($\Delta V \approx 4.43$ eV) across the interface, confirming the formation of an interfacial dipole. The offset between the potential plateaus of g-C_3N_4 and CeO_2 reflects their intrinsic energy level alignment and corroborates the type-II band alignment, as discussed earlier. As summarized in Table 1, this alignment facilitates spatial separation of charge carriers, thereby enhancing the interfacial photocatalytic efficiency, consistent with our experimental observations.

Table 1. Key DFT Data for $CeO_2(110)$, g-C_3N_4, and the $CeO_2(110)/g\text{-}C_3N_4$ Heterostructure[a]

system	VBM (eV)	CBM (eV)	Band gap (eV)	type of the band gap	ΔV (eV)
CeO_2 (110)	−0.74	0.66	1.40	direct	
g-C_3N_4	−1.12	0.88	2.00	indirect (K−Γ)	
$CeO_2(110)/g\text{-}C_3N_4$	−0.08	0.23	0.31[b]	type-II	∼4.43

[a]The VBM and CBM values are referenced to their respective Fermi levels. ΔV denotes the interfacial electrostatic potential step extracted from the plane-averaged and macroscopic-averaged potential profiles. [b]Interfacial band gap derived from the staggered band alignment in the heterostructure between the VBM dominated by CeO_2 and the g-C_3N_4 CBM.

4. CONCLUSION

To recapitulate, we have introduced an innovative strategy to design heterostructured catalysts by incorporating CeO_2 nanocubes onto GCN nanosheets for enhanced PEC and photocatalytic hydrogen generation. The optimal nanohybrid has demonstrated a significantly improved photocurrent of 5.70 mAcm^{-2} at a very low onset potential and achieved a high H_2 production rate of 809.23 μmol g^{-1} h^{-1}, outperforming both pure CeO_2 and GCN. This outstanding performance is attributed to the synergistic interaction between CeO_2 and GCN, which reduces recombination of photoinduced charge carriers and provides a higher number of reactive sites for driving the water splitting reaction. The findings show that the effective separation of charge carriers through the interface significantly contributes to the enhanced photoactivity and high stability of the catalyst. Further, the improved optical and electronic properties of the nanohybrid have also contributed to the enhancement, as evidenced by the DFT calculations and the FDTD simulation. The synthesized heterojunctions have exhibited excellent stability over three consecutive cycles of photocatalytic hydrogen production, with negligible activity loss. The FDTD study and the electronic structure calculations have validated the experimental results, offering valuable insights into the modified band structure and optical response at the interface. This work demonstrates that the strategic construction of heterojunctions can effectively promote the water splitting reactions, moving toward carbon-free fuels in the future energy economy.

■ ASSOCIATED CONTENT

Supporting Information

The Supporting Information is available free of charge at https://pubs.acs.org/doi/10.1021/acsami.5c10272.

Characterization of the samples; photocatalytic hydrogen evolution test; photoelectrochemical experiment details; zeta potential of GCN and CeO_2; pH versus zeta potential plot; SEM image of the samples; EDS image and elemental mapping; deconvoluted PL peak; and optimized atomic geometry of the heterostructure (PDF)

■ AUTHOR INFORMATION

Corresponding Authors

Abinash Das − *Solar Fuel Research Group (SFRG), PSG Institute of Advanced Studies, Coimbatore, Tamil Nadu 641004, India;* orcid.org/0000-0001-7715-2617; Email: abinashnitsmsc@gmail.com

https://doi.org/10.1021/acsami.5c10272
ACS Appl. Mater. Interfaces XXXX, XXX, XXX−XXX

Shashi B. Mishra − *Department of Physics and Astronomy, Binghamton University-SUNY, New York, New York 13902, United States;* orcid.org/0000-0002-6361-3379; Email: mshashi125@gmail.com

Oleg V. Prezhdo − *Department of Chemistry, University of Southern California, Los Angeles, California 90089, United States; Department of Physics & Astronomy, University of Southern California, Los Angeles, California 90089, United States;* orcid.org/0000-0002-5140-7500; Email: prezhdo@usc.edu

Authors

Shriya Gumber − *Department of Chemistry, University of Southern California, Los Angeles, California 90089, United States*

Nitai C. Maji − *Department of Chemical Engineering and Technology, Indian Institute of Technology (BHU), Varanasi 221005, India;* orcid.org/0000-0001-6405-6853

Preethi M. − *Solar Fuel Research Group (SFRG), PSG Institute of Advanced Studies, Coimbatore, Tamil Nadu 641004, India*

Pujita Ningthoukhongjam − *Solar Energy Materials Research and Testing Laboratory, Department of Physics, National Institute of Technology Silchar, Silchar, Cachar, Assam 785001, India*

Ranjith G. Nair − *Solar Energy Materials Research and Testing Laboratory, Department of Physics, National Institute of Technology Silchar, Silchar, Cachar, Assam 785001, India;* orcid.org/0000-0002-1780-3024

Abhijith T. − *Department of Physics, PSG Institute of Technology and Applied Research, Coimbatore, Tamil Nadu 641062, India; Department of Nanoscience and Technology, PSG Institute of Advanced Studies, Coimbatore, Tamil Nadu 641004, India;* orcid.org/0000-0001-5152-4478

Elena A. Kazakova − *Department of Biochemistry, Sechenov First Moscow State Medical University, Moscow 119991, Russia*

Andrey S. Vasenko − *HSE University, Moscow 101000, Russia; Donostia International Physics Center (DIPC), San Sebastián-Donostia 20018, Spain;* orcid.org/0000-0002-2978-8650

Madhumitha R. − *Solar Fuel Research Group (SFRG), PSG Institute of Advanced Studies, Coimbatore, Tamil Nadu 641004, India*

Complete contact information is available at: https://pubs.acs.org/10.1021/acsami.5c10272

Notes

The authors declare no competing financial interest.

■ ACKNOWLEDGMENTS

A.D. is grateful for the support provided by the UGC-DAE CSR (CRS/2024-25/02/1505). A.S.V. acknowledges support from the project "International academic cooperation" of HSE University. O.V.P. acknowledges funding of the US Department of Energy (DE-SC0014429). S.B.M. acknowledges the Texas Advanced Computing Center (TACC) at UT Austin (http://www.tacc.utexas.edu) for providing computational resources through the ACCESS program under Award No. TG-PHY250052. S.B.M. also thanks B. Biswal for assistance in the design of the heterostructure.

■ REFERENCES

(1) Rafique, M.; Hajra, S.; Irshad, M.; Usman, M.; Imran, M.; Assiri, M. A.; Ashraf, W. M. Hydrogen Production Using TiO2-Based Photocatalysts: A Comprehensive Review. *ACS Omega* **2023**, *8* (29), 25640−25648.

(2) Corredor, J.; Rivero, M. J.; Rangel, C. M.; Gloaguen, F.; Ortiz, I. Comprehensive Review and Future Perspectives on the Photocatalytic Hydrogen Production. *J. Chem. Technol. Biotechnol.* **2019**, *94* (10), 3049−3063.

(3) Chen, X.; Shen, S.; Guo, L.; Mao, S. S. Semiconductor-Based Photocatalytic Hydrogen Generation. *Chem. Rev.* **2010**, *110* (11), 6503−6570.

(4) Thakur, A.; Chand, H.; Thakur, S.; Kumar, A. Production of Green Hydrogen by Photocatalysis: Basic Process and Mechanism. *Towards Sustainable and Green Hydrogen Production by Photocatalysis: Scalability Opportunities and Challenges (Vol. 1)*; *ACS Symposium Series*; American Chemical Society, 2024; Vol. *1467*; pp 1−25.

(5) Acar, C.; Dincer, I.; Zamfirescu, C. A Review on Selected Heterogeneous Photocatalysts for Hydrogen Production. *Int. J. Energy Res.* **2014**, *38* (15), 1903−1920.

(6) Chu, J.; Sun, Y.; Han, X.; Zhang, B.; Du, Y.; Song, B.; Xu, P. Mixed Titanium Oxide Strategy for Enhanced Photocatalytic Hydrogen Evolution. *ACS Appl. Mater. Interfaces* **2019**, *11* (20), 18475−18482.

(7) Kumar, M.; Singh, N. K.; Kumar, R. S.; Singh, R. Production of Green Hydrogen through Photocatalysis. *Towards Sustainable and Green Hydrogen Production by Photocatalysis: Insights into Design and Development of Efficient Materials (Vol. 2)*; *ACS Symposium Series*; American Chemical Society, 2024; Vol. *1468*; pp 1−24.

(8) Cao, S.; Yu, J. G-C3N4-Based Photocatalysts for Hydrogen Generation. *J. Phys. Chem. Lett.* **2014**, *5* (12), 2101−2107.

(9) Liu, W.; Zhang, D.; Wang, R.; Zhang, Z.; Qiu, S. 2D/2D Interface Engineering Promotes Charge Separation of Mo2C/g-C3N4 Nanojunction Photocatalysts for Efficient Photocatalytic Hydrogen Evolution. *ACS Appl. Mater. Interfaces* **2022**, *14* (28), 31782−31791.

(10) Zhu, Q.; Xu, Z.; Qiu, B.; Xing, M.; Zhang, J. Emerging Cocatalysts on G-C3N4 for Photocatalytic Hydrogen Evolution. *Small* **2021**, *17* (40), 2101070.

(11) Bhanderi, D.; Lakhani, P.; Modi, C. K. Graphitic Carbon Nitride (g-C3N4) as an Emerging Photocatalyst for Sustainable Environmental Applications: A Comprehensive Review. *RSC Sustainability* **2024**, *2* (2), 265−287.

(12) Ong, W.-J.; Tan, L.-L.; Ng, Y. H.; Yong, S.-T.; Chai, S.-P. Graphitic Carbon Nitride (g-C3N4)-Based Photocatalysts for Artificial Photosynthesis and Environmental Remediation: Are We a Step Closer To Achieving Sustainability? *Chem. Rev.* **2016**, *116* (12), 7159−7329.

(13) Fu, J.; Yu, J.; Jiang, C.; Cheng, B. G-C3N4-Based Heterostructured Photocatalysts. *Adv. Energy Mater.* **2018**, *8* (3), 1701503.

(14) Hayat, A.; Sohail, M.; Anwar, U.; Taha, T. A.; Qazi, H. I. A.; Amina; Ajmal, Z.; Al-Sehemi, A. G.; Algarni, H.; Al-Ghamdi, A. A.; Amin, M. A.; Palamanit, A.; Nawawi, W. I.; Newair, E. F.; Orooji, Y. A Targeted Review of Current Progress, Challenges and Future Perspective of g-C3N4 Based Hybrid Photocatalyst Toward Multi-dimensional Applications. *Chem. Rec.* **2023**, *23* (1), No. e202200143.

(15) Zhang, M.; Yang, Y.; An, X.; Hou, L. A Critical Review of G-C3N4-Based Photocatalytic Membrane for Water Purification. *Chem. Eng. J.* **2021**, *412*, 128663.

(16) Luo, Y.; Zhu, Y.; Han, Y.; Ye, H.; Liu, R.; Lan, Y.; Xue, M.; Xie, X.; Yu, S.; Zhang, L.; Yin, Z.; Gao, B. G-C3N4-Based Photocatalysts for Organic Pollutant Removal: A Critical Review. *Carbon Res.* **2023**, *2* (1), 14.

(17) Chen, L.; Maigbay, M. A.; Li, M.; Qiu, X. Synthesis and Modification Strategies of G-C3N4 Nanosheets for Photocatalytic Applications. *Adv. Powder Mater.* **2024**, *3* (1), 100150.

(18) Das, S.; Deka, T.; Ningthoukhangjam, P.; Chowdhury, A.; Nair, R. G. A Critical Review on Prospects and Challenges of Metal-Oxide Embedded g-C3N4-Based Direct Z-Scheme Photocatalysts for Water

Splitting and Environmental Remediation. *Appl. Surf. Sci. Adv.* **2022**, *11*, 100273.
(19) Wei, L.-W.; Liu, S.-H.; Wang, H. P. Visible-Light Photocatalytic CO2-to-CO and H2O-to-H2O2 by g-C3N4/Cu2O−Pd S-Scheme Heterojunctions. *ACS Appl. Mater. Interfaces* **2023**, *15* (21), 25473−25483.
(20) Aboubakr, A. E. A.; Hussien, M. K.; Sabbah, A.; Hassan, A. E.; Elsayed, M. H.; Wen, Z.; Chen, K.-H.; Hung, C.-H. Direct Z-Scheme Heterostructure of In Situ Planted ZnO Nanorods on g-C_3 N_4 Thin Sheets Sprayed on TiO_2 Layer: A Strategy for Ternary-Photoanode Engineering toward Enhanced Photoelectrochemical Water Splitting. *ACS Appl. Energy Mater.* **2024**, *7* (3), 906−918.
(21) Kwon, N. H.; Park, J.; Jin, X.; Kim, S.-J.; Kim, H.; Hwang, S.-J. Defect-Regulated Two-Dimensional Superlattice of Holey g-C_3 N_4 − TiO_2 Nanohybrids: Contrasting Influence of Vacancy Content on Hybridization Impact and Photocatalyst Performance. *ACS Nano* **2023**, *17* (23), 23732−23745.
(22) Pham, V. V.; Truong, T. K.; Hai, L. V.; La, H. P. P.; Nguyen, H. T.; Lam, V. Q.; Tong, H. D.; Nguyen, T. Q.; Sabbah, A.; Chen, K.-H.; You, S.-J.; Cao, T. M. S-Scheme α-Fe_2 O_3/g-C_3 N_4 Nanocomposites as Heterojunction Photocatalysts for Antibiotic Degradation. *ACS Appl. Nano Mater.* **2022**, *5* (3), 4506−4514.
(23) Shen, R.; Zhang, L.; Li, N.; Lou, Z.; Ma, T.; Zhang, P.; Li, Y.; Li, X. W−N Bonds Precisely Boost Z-Scheme Interfacial Charge Transfer in g-C_3 N_4/WO_3 Heterojunctions for Enhanced Photocatalytic H_2 Evolution. *ACS Catal.* **2022**, *12* (16), 9994−10003.
(24) Yan, Y.-Q.; Wu, Y.-Z.; Wu, Y.-H.; Weng, Z.-L.; Liu, S.-J.; Liu, Z.-G.; Lu, K.-Q.; Han, B. Recent Advances of CeO2-Based Composite Materials for Photocatalytic Applications. *ChemSusChem* **2024**, *17* (14), No. e202301778.
(25) Cai, J.; Li, D.; Jiang, L.; Yuan, J.; Li, Z.; Li, K. Review on CeO2-Based Photocatalysts for Photocatalytic Reduction of CO2: Progresses and Perspectives. *Energy Fuels* **2023**, *37* (7), 4878−4897.
(26) Li, Q.; Song, L.; Liang, Z.; Sun, M.; Wu, T.; Huang, B.; Luo, F.; Du, Y.; Yan, C.-H. A Review on Ceo2-Based Electrocatalyst and Photocatalyst in Energy Conversion. *Adv. Energy Sustainability Res.* **2021**, *2* (2), 2000063.
(27) Ahmad, I.; Shukrullah, S.; Naz, M. Y.; Alsaif, F. K.; Alsulamy, S.; Khan, Y.; Khalid, N. R.; Khan, W. Q. Construction of Ag-Modified ZnO−CeO2 2D-1D S-Scheme Heterojunction Photocatalyst with Phenomenal Photocatalytic Performance for H2 Evolution. *Mater. Sci. Semicond. Process.* **2023**, *159*, 107392.
(28) Bhargava, R.; Shah, J.; Khan, S.; Kotnala, R. K. Hydroelectric Cell Based on a Cerium Oxide-Decorated Reduced Graphene Oxide (CeO2−rG) Nanocomposite Generates Green Electricity by Room-Temperature Water Splitting. *Energy Fuels* **2020**, *34* (10), 13067−13078.
(29) Wang, Y.; Zou, J.; Zhao, C.; Jiang, H.; Song, Y.; Zhang, L.; Li, X.; Wang, F.; Fan, L.; Liu, X.; Wei, M.; Yang, L. Building a Charge Transfer Bridge between G-C3N4 and Perovskite with Molecular Engineering to Achieve Efficient Perovskite Solar Cells. *ACS Appl. Mater. Interfaces* **2024**, *16* (11), 13815−13827.
(30) Bhandari, S.; Valsalakumar, S.; Ali, M. S.; Mallick, T. K.; Hinshelwood, J.; Sundaram, S. Influence of Adjustable CeO2Morphology on the Performance of Ambient Hole Transport Layer-Free Carbon-Based Perovskite Solar Cells. *Energy Fuels* **2025**, *39* (20), 9566−9575.
(31) Liu, X.; He, L.; Chen, X.; Du, L.; Gu, X.; Wang, S.; Fu, M.; Dong, F.; Huang, H. Facile Synthesis of CeO2/g-C3N4 Nanocomposites with Significantly Improved Visible-Light Photocatalytic Activity for Hydrogen Evolution. *Int. J. Hydrogen Energy* **2019**, *44* (31), 16154−16163.
(32) Ma, R.; Zhang, S.; Li, L.; Gu, P.; Wen, T.; Khan, A.; Li, S.; Li, B.; Wang, S.; Wang, X. Enhanced Visible-Light-Induced Photoactivity of Type-II CeO2/g-C3N4 Nanosheet toward Organic Pollutants Degradation. *ACS Sustainable Chem. Eng.* **2019**, *7* (10), 9699−9708.
(33) Chauhan, H.; Gupta, R. Photocatalytic Dye Degradation of Rhodamine B and Congo Red Dye Using Sulfur Doped Graphitic Carbon Nitride and Cerium Oxide Nanocomposite. *J. Water Process Eng.* **2025**, *75*, 108052.
(34) Kumar, A.; Arya, V.; Pathak, A.; Trivedi, S.; Guin, D.; Tripathi, C. S. P. Enhanced Visible Light Photocatalytic Performance of CeO2@Acidified G-C3N4 Nanoheterostructures for RhB Degradation. *Langmuir* **2025**, *41* (23), 14765−14777.
(35) Feng, C.; Rong, J.; Zhang, Y.; Zheng, X.; Li, X.; Xu, S.; Li, Z. An S-Scheme CeO2/Foveolate g-C3N4 Composite with Horseradish Peroxidase Activity for Photo-Enzyme Synergistic Catalytic Degradation of Phenanthrene. *Appl. Catal., B* **2023**, *337*, 123005.
(36) Das, A.; Liu, D.; Wu, Y.; Abzakh, B. A.; R, M.; M, P.; Kazakova, E. A.; Vasenko, A. S.; Prezhdo, O. V. Origin of the Improved Photoelectrochemical and Photocatalytic Activity in a ZnO-TiO_2 Nanohybrid Revealed by Experimental and Density Functional Theory Studies. *J. Phys. Chem. Lett.* **2024**, *15* (29), 7524−7532.
(37) Xu, Q.; Zhu, B.; Jiang, C.; Cheng, B.; Yu, J. Constructing 2D/2D Fe_2 O_3/g-C_3 N_4 Direct Z-Scheme Photocatalysts with Enhanced H_2 Generation Performance. *Sol. RRL* **2018**, *2* (3), 1800006.
(38) Chen, J.; Xu, X.; Li, T.; Pandiselvi, K.; Wang, J. Toward High Performance 2D/2D Hybrid Photocatalyst by Electrostatic Assembly of Rationally Modified Carbon Nitride on Reduced Graphene Oxide. *Sci. Rep.* **2016**, *6* (1), 37318.
(39) Liu, D.; Wang, B.; Wu, Y.; Vasenko, A. S.; Prezhdo, O. V. Breaking the Size Limitation of Nonadiabatic Molecular Dynamics in Condensed Matter Systems with Local Descriptor Machine Learning. *Proc. Natl. Acad. Sci. U.S.A.* **2024**, *121* (36), No. e2403497121.
(40) Ran, J.; Wang, B.; Wu, Y.; Liu, D.; Mora Perez, C.; Vasenko, A. S.; Prezhdo, O. V. Halide Vacancies Create No Charge Traps on Lead Halide Perovskite Surfaces but Can Generate Deep Traps in the Bulk. *J. Phys. Chem. Lett.* **2023**, *14* (26), 6028−6036.
(41) Zhao, X.; Vasenko, A. S.; Prezhdo, O. V.; Long, R. Anion Doping Delays Nonradiative Electron−Hole Recombination in Cs-Based All-Inorganic Perovskites: Time Domain Ab Initio Analysis. *J. Phys. Chem. Lett.* **2022**, *13* (49), 11375−11382.
(42) Giannozzi, P.; Andreussi, O.; Brumme, T.; Bunau, O.; Buongiorno Nardelli, M.; Calandra, M.; Car, R.; Cavazzoni, C.; Ceresoli, D.; Cococcioni, M.; Colonna, N.; Carnimeo, I.; Dal Corso, A.; de Gironcoli, S.; Delugas, P.; DiStasio, R. A.; Ferretti, A.; Floris, A.; Fratesi, G.; Fugallo, G.; Gebauer, R.; Gerstmann, U.; Giustino, F.; Gorni, T.; Jia, J.; Kawamura, M.; Ko, H.-Y.; Kokalj, A.; Küçükbenli, E.; Lazzeri, M.; Marsili, M.; Marzari, N.; Mauri, F.; Nguyen, N. L.; Nguyen, H.-V.; Otero-de-la-Roza, A.; Paulatto, L.; Poncé, S.; Rocca, D.; Sabatini, R.; Santra, B.; Schlipf, M.; Seitsonen, A. P.; Smogunov, A.; Timrov, I.; Thonhauser, T.; Umari, P.; Vast, N.; Wu, X.; Baroni, S. Advanced Capabilities for Materials Modelling with Quantum ESPRESSO. *J. Phys.: Condens. Matter* **2017**, *29* (46), 465901.
(43) Perdew, J. P.; Burke, K.; Ernzerhof, M. Generalized Gradient Approximation Made Simple. *Phys. Rev. Lett.* **1996**, *77* (18), 3865−3868.
(44) Topsakal, M.; Wentzcovitch, R. M. Accurate Projected Augmented Wave (PAW) Datasets for Rare-Earth Elements (RE = La−Lu). *Comput. Mater. Sci.* **2014**, *95*, 263−270.
(45) Cococcioni, M.; de Gironcoli, S. Linear Response Approach to the Calculation of the Effective Interaction Parameters in the $ \mathrm{LDA}+\mathrm{U}$ Method. *Phys. Rev. B* **2005**, *71* (3), 035105.
(46) Mishra, S. B.; Roy, S. C.; Nanda, B. R. K. Electronic Structure of Graphene/TiO2 Interface: Design and Functional Perspectives. *Appl. Surf. Sci.* **2021**, *542*, 148709.
(47) Sahoo, P.; Mishra, S. B.; Debata, S.; Sharma, A.; Sahu, B. K.; Padhan, S.; Thangavel, R.; Lee, B.-K. Hydrothermally Grown Halogen-Doped ZnO Nanorods for Photoelectrochemical Water Oxidation: Experimental and DFT Insights. *J. Phys. Chem. C* **2024**, *128* (44), 18711−18723.
(48) Cheng, Z.; Sherman, B. J.; Lo, C. S. Carbon Dioxide Activation and Dissociation on Ceria (110): A Density Functional Theory Study. *J. Chem. Phys.* **2013**, *138* (1), 014702.
(49) Hezam, A.; Namratha, K.; Drmosh, Q. A.; Ponnamma, D.; Wang, J.; Prasad, S.; Ahamed, M.; Cheng, C.; Byrappa, K. CeO_2

https://doi.org/10.1021/acsami.5c10272
ACS Appl. Mater. Interfaces XXXX, XXX, XXX−XXX

Nanostructures Enriched with Oxygen Vacancies for Photocatalytic CO_2 Reduction. *ACS Appl. Nano Mater.* **2020**, *3* (1), 138−148.
(50) Castleton, C. W. M.; Kullgren, J.; Hermansson, K. Tuning LDA +U for Electron Localization and Structure at Oxygen Vacancies in Ceria. *J. Chem. Phys.* **2007**, *127* (24), 244704.
(51) Stradi, D.; Jelver, L.; Smidstrup, S.; Stokbro, K. Method for Determining Optimal Supercell Representation of Interfaces. *J. Phys.: Condens. Matter* **2017**, *29* (18), 185901.
(52) Loschen, C.; Carrasco, J.; Neyman, K. M.; Illas, F. First-Principles $\mathrm{LDA}+\mathrm{U}$ and $\mathrm{GGA}+\mathrm{U}$ Study of Cerium Oxides: Dependence on the Effective U Parameter. *Phys. Rev. B* **2007**, *75* (3), 035115.
(53) Vu, M. H.; Nguyen, C. C.; Do, T.-O. Graphitic Carbon Nitride (g-C3N4) Nanosheets as a Multipurpose Material for Detection of Amines and Solar-Driven Hydrogen Production. *ChemPhotoChem* **2021**, *5* (5), 466−475.
(54) Chang, F.; Xie, Y.; Li, C.; Chen, J.; Luo, J.; Hu, X.; Shen, J. A Facile Modification of *g*-C3N4 with Enhanced Photocatalytic Activity for Degradation of Methylene Blue. *Appl. Surf. Sci.* **2013**, *280*, 967−974.
(55) Fang, S.; Xia, Y.; Lv, K.; Li, Q.; Sun, J.; Li, M. Effect of Carbon-Dots Modification on the Structure and Photocatalytic Activity of g-C3N4. *Appl. Catal., B* **2016**, *185*, 225−232.
(56) Tan, L.; Xu, J.; Zhang, X.; Hang, Z.; Jia, Y.; Wang, S. Synthesis of G-C3N4/CeO2 Nanocomposites with Improved Catalytic Activity on the Thermal Decomposition of Ammonium Perchlorate. *Appl. Surf. Sci.* **2015**, *356*, 447−453.
(57) Li, C.; Du, Y.; Wang, D.; Yin, S.; Tu, W.; Chen, Z.; Kraft, M.; Chen, G.; Xu, R. Unique P Co N Surface Bonding States Constructed on G-C3N4 Nanosheets for Drastically Enhanced Photocatalytic Activity of H2 Evolution. *Adv. Funct. Mater.* **2017**, *27* (4), 1604328.
(58) Maslakov, K. I.; Teterin, Y. A.; Popel, A. J.; Teterin, A. Yu.; Ivanov, K. E.; Kalmykov, S. N.; Petrov, V. G.; Petrov, P. K.; Farnan, I. XPS Study of Ion Irradiated and Unirradiated CeO2 Bulk and Thin Film Samples. *Appl. Surf. Sci.* **2018**, *448*, 154−162.
(59) Sungu Akdogan, C. Z.; Gokcal, B.; Polat, M.; Hamaloglu, K. O.; Kip, C.; Tuncel, A. Porous, Oxygen Vacancy Enhanced CeO_{2-x} Microspheres with Efficient Enzyme-Mimetic and Photothermal PropertiesVacancy Enhanced CeO_{2-x} Microspheres with Efficient Enzyme-Mimetic and Photothermal Properties. *ACS Sustainable Chem. Eng.* **2022**, *10* (29), 9492−9505.
(60) Zhang, S.; Guo, J.; Zhang, W.; Gao, H.; Huang, J.; Chen, G.; Xu, X. Dopant and Defect Doubly Modified CeO2/g-C3N4 Nanosheets as 0D/2D Z-Scheme Heterojunctions for Photocatalytic Hydrogen Evolution: Experimental and Density Functional Theory Studies. *ACS Sustainable Chem. Eng.* **2021**, *9* (34), 11479−11492.
(61) Bharathi, R. N.; Sankar, S. Investigation of Transport Properties of Pr Doped Cerium Oxide Nanoparticles as a Solid Electrolyte for IT-SOFC Applications. *J. Inorg. Organomet. Polym.* **2018**, *28* (5), 1829−1838.
(62) Riyajuddin, S.; Kumar, S.; Gaur, S. P.; Sud, A.; Maruyama, T.; Ali, M. E.; Ghosh, K. Linear Piezoresistive Strain Sensor Based on Graphene/g-C3N4/PDMS Heterostructure. *Nanotechnology* **2020**, *31* (29), 295501.
(63) de Castro Silva, I.; Sigoli, F. A.; Mazali, I. O. Reversible Oxygen Vacancy Generation on Pure CeO2 Nanorods Evaluated by in Situ Raman Spectroscopy. *J. Phys. Chem. C* **2017**, *121* (23), 12928−12935.
(64) Qu, L.; Wang, N.; Xu, H.; Wang, W.; Liu, Y.; Kuo, L.; Yadav, T. P.; Wu, J.; Joyner, J.; Song, Y.; Li, H.; Lou, J.; Vajtai, R.; Ajayan, P. M. Gold Nanoparticles and G-C3N4-Intercalated Graphene Oxide Membrane for Recyclable Surface Enhanced Raman Scattering. *Adv. Funct. Mater.* **2017**, *27* (31), 1701714.
(65) Yang, Z.; Xiang, X.; Yang, J.; Zhao, Z.-Y. High-Entropy Oxides as Energy Materials: From Complexity to Rational Design. *Mater. Futures* **2024**, *3* (4), 042103.
(66) Xin, G.; Meng, Y. Pyrolysis Synthesized G-C3N4 for Photocatalytic Degradation of Methylene Blue. *J. Chem.* **2013**, *2013* (1), 187912.
(67) Boonprakob, N.; Wetchakun, N.; Phanichphant, S.; Waxler, D.; Sherrell, P.; Nattestad, A.; Chen, J.; Inceesungvorn, B. Enhanced Visible-Light Photocatalytic Activity of g-C3N4/TiO2 Films. *J. Colloid Interface Sci.* **2014**, *417*, 402−409.
(68) Li, R.; Gao, T.; Wang, Y.; Chen, Y.; Luo, W.; Wu, Y.; Xie, Y.; Wang, Y.; Zhang, Y. Engineering of Bimetallic Au−Pd Alloyed Particles on Nitrogen Defects Riched g-C3N4 for Efficient Photocatalytic Hydrogen Production. *Int. J. Hydrogen Energy* **2024**, *63*, 1116−1127.
(69) Ganesan, S.; Kokulnathan, T.; Sumathi, S.; Palaniappan, A. Efficient Photocatalytic Degradation of Textile Dye Pollutants Using Thermally Exfoliated Graphitic Carbon Nitride (TE−g−C3N4). *Sci. Rep.* **2024**, *14* (1), 2284.
(70) Das, S.; Pramanik, S.; Nair, R. G.; Chowdhury, A. Heterointerface Engineering in Mesoporous G-C3N4@MnFe2O4 Photocatalysts for Superior Hydrogen (H2) Evolution. *Surf. Interfaces* **2024**, *54*, 105226.
(71) Skorodumova, N. V.; Baudin, M.; Hermansson, K. Surface Properties of ${\mathrm{CeO}}_{2}$ from First Principles. *Phys. Rev. B* **2004**, *69* (7), 075401.
(72) Alekseev, R. F.; Saraev, A. A.; Kurenkova, A. Y.; Kozlova, E. A. Heterostructures Based on G-C3N4 for the Photocatalytic CO2 Reduction. *Russ. Chem. Rev.* **2024**, *93* (5), RCR5124.
(73) Wang, X.; Maeda, K.; Thomas, A.; Takanabe, K.; Xin, G.; Carlsson, J. M.; Domen, K.; Antonietti, M. A Metal-Free Polymeric Photocatalyst for Hydrogen Production from Water under Visible Light. *Nat. Mater.* **2009**, *8* (1), 76−80.
(74) Samanta, S.; Mishra, S. B.; Nanda, B. R. K. Quantum Well Structure of a Double Perovskite Superlattice and Formation of a Spin-Polarized Two-Dimensional Electron Gas. *Phys. Rev. B* **2018**, *98* (11), 115155.
(75) Yalavarthi, R.; B Mishra, S.; Henrotte, O.; Cortes, E. Defects Dynamic in Photo-Excited CeO_2 and Their Influence on CO_2 Photoreduction. *Adv. Funct. Mater.* **2025**, No. e13933.

https://doi.org/10.1021/acsami.5c10272
ACS Appl. Mater. Interfaces XXXX, XXX, XXX−XXX